Journal of Energy

VOLUME 63 | 2014

journal homepage: http://journalofenergy.com/

Ralf Wittmaack
Siemens AG, Nürnberg, Germany
Ralf.Wittmaack@Siemens.com

CFD SIMULATION OF PRESSURE LOSS IN HVDC TRANSFORMER WINDING

SUMMARY

At Siemens the in-house CFD code UniFlow is used to analyse fluid flow and heat transfer in oil-immersed and dry-type transformers, as well as transformer components like windings, cores, tank walls, and radiators. It can be employed to perform steady state as well as transient analyses. This paper describes its physical models and numerical solution methods.

Moreover, it presents an application to a valve winding of a HVDC transformer, cooled by mineral oil. This study is aimed at finding the flow induced pressure loss in the winding and the static ring assembly below and above the winding. The investigation includes isothermal runs with different inlet velocity and a conjugate heat transfer run with a conductor representation.

In the isothermal simulations a steady state is established and the pressure loss is an almost linear function of the inlet velocity. In the run involving heat transfer, the high buoyancy forces hamper the development of a steady state and the possibility to calculate a flow induced pressure loss.

Key words: Thermal design, CFD, pressure loss, physical models, numerical methods

1. INTRODUCTION

Thanks to its flexibility and accuracy, CFD (Computational Fluid Dynamics) is increasingly being used to analyse transformer thermal design. This follows the trend established in other branches of advanced technology development like aerospace, automotive, and power generation, where CFD simulations are indispensable parts of the product development cycles.

Employing commercial CFD codes, several detailed studies of disc-type transformer windings were performed, e.g., by [1] and [2]. Moreover, extended full geometry CFD analyses coupled to electrodynamic simulation of the load and no-load losses in core and windings were presented, e.g., by [3], [4]. Furthermore, combined oil and air flows in fin-type distribution transformers were investigated with commercial CFD codes, e.g., by [5], [6].

Our intention is to provide a simulation method that may be used for detailed CFD analyses on fine grids as well as for simplified coarse grid studies. The in-house code UniFlow is designed to be applicable also by users with limited experience in CFD. For this reason, e.g., material attributes are employed for a convenient coupling of fluid and solid regions in conjugate heat transfer simulations.

2. PHYSICAL MODELS AND NUMERICAL METHODS

2.1. Physical models

Our physical model is aimed at investigating flows with several kinds of heat transfer in a complex geometry. It simulates the flow of single-component, incompressible, Newtonian fluids in a three-dimensional geometry. In addition to the fluids, that may be in gaseous or liquid state, several structural materials are considered as hydrodynamic obstacles and thermodynamic heat structures. The hydrodynamics is described by the continuity and the Navier-Stokes equation. For the simulation of turbulence the algebraic Baldwin-Lomax eddy viscosity model [7] is available. To simulate the transition between laminar and turbulent flows, algebraic transition models of Drela [8] and Mayle [9] are on hand.

For temperature dependent density or material properties of the viscous stress tensor, the hydrodynamics of the fluid is coupled to the thermodynamics. For this reason, internal heat transfer (by convection and conduction) and heat generation by internal sources as well as heat transfer to the surroundings are modelled via a heat transport equation. To allow for the simulation of phase transitions it is provided in enthalpy formulation. At the rigid boundaries heat conduction is considered. For coarse grids convective heat transfer coefficients may be employed at solid-liquid interfaces. Radiant heat transfer is simulated at structural material surfaces. The material properties (density, dynamic viscosity, specific heat at constant pressure, heat conductivity, and convective heat transfer coefficient) depend on the temperature. Solids may have orthotropic heat conductivity.

2.1.1. Dynamic equations

Our dynamic equations are written in Cartesian coordinates. The continuity equation for incompressible flow is [10]

$$\frac{\partial}{\partial x^m}\left(\rho\, v^m\right) = 0 \ , \tag{1}$$

where ρ is density and v velocity. x are the space coordinates and we use Einstein's summation convention for the space direction index m. Introduction of the continuity equation into the Navier-Stokes equation [10] leads to a momentum equation in strong conservation form

$$\rho\frac{\partial v_i}{\partial t} + \frac{\partial}{\partial x^m}\left[\rho\, v_i\, v^m - \mu\left(\frac{\partial v_i}{\partial x_m} + \frac{\partial v^m}{\partial x^i}\right)\right] = -\frac{\partial p}{\partial x^i} + \rho\, g_i \ , \tag{2}$$

where t is time, p pressure, and g gravitational acceleration. After inclusion of the continuity equation our heat transport equation in strong conservation form reads

$$\rho\frac{\partial h}{\partial t} + \frac{\partial}{\partial x^m}\left(\rho\, h\, v^m - \lambda\frac{\partial T}{\partial x_m}\right) = P_d \ . \tag{3}$$

Here h is specific enthalpy, T temperature, λ heat conductivity, and P_d density of the heat sources or sinks.

2.1.2. Radiant heat transfer model

Radiant heat transfer may be simulated between structural material surfaces adjacent to the fluid. The employed radiation model assumes that the radiating surfaces are boundaries of a hollow space with linear dimension much greater than their distance. It is applicable for, e.g., parallel plates and concentric cylinders. With this simplifying assumption the power received by surface 'a' via the heat transfer from surface 'b' is [11]

$$P_{ab} = c_{ab}\ A_a \left(T_b^4 - T_a^4\right);\ c_{ab} := \frac{\sigma}{\frac{1}{\varepsilon_a} + \frac{A_a}{A_b}\left(\frac{1}{\varepsilon_b} - 1\right)}\ . \quad (4)$$

Here A is area of radiating structural material, T surface temperature, σ = 5.67051*10^{-8} W/(m^2 K^4) Stefan-Boltzmann constant, and ε emissivity of a structural material surface. Computation domain nodes undergoing radiant heat transfer may have their radiation partner nodes inside the computation domain or at the boundary.

2.2. Numerical methods

For the numerical representation of our model we developed a finite volume method and employ boundary fitted, curvilinear, non-orthogonal, block-structured grids. The blocks may be connected via 1-to-1 or patched couplings. The arrangement of the dynamic variables in the control volumes of the grid is collocated at the node centre. The dynamic equations are solved sequentially. For the solution of the momentum, pressure-correction, and heat transport equations we use implicit schemes. The system of continuity and momentum equations is solved by a SIMPLE [12], SIMPLEC [13], or PISO [14] algorithm.

To speed up the code execution and to simplify the estimation of discretisation errors a FAS multi-grid algorithm is employed [15]. It is a geometric approach with standard coarsening applied to the outer iterations, visiting the grid levels in V-cycles. For steady-state problems it operates as a full multi-grid algorithm (FMG), whereas for transient problems the algorithm starts at the finest grid.

For the efficient solution of sparse linear equations several algorithms are available. The parabolic momentum and heat transport equations may be solved with SIP solvers that are modified to handle block couplings via the residual vector [12]. Additionally, for the elliptic pressure-correction equation an aggregation-based algebraic multi-grid algorithm [16] is available.

The UniFlow source code is written in C++. For multi-threaded shared memory parallelism, OpenMP is employed. In addition, for distributed memory parallelisation MPI is used.

3. APPLICATION TO PRESSURE LOSS IN WINDING OF HVDC TRANSFORMER

In this section we analyse the pressure loss in the valve winding of a HVDC transformer cooled by mineral oil. We consider natural convection of the oil, i.e., the ON cooling mode. As only a part of the natural convection loop is simulated, we employ in- and outlet boundary conditions at the entry and exit to the labyrinth.

3.1. Geometry model

Our geometry model covers the winding and its system of static rings below and above the winding. We simplify the geometry of the oil regions in the labyrinths by removing those outer parts that provide a negligible contribution to the oil flow. Furthermore, the winding geometry is simplified by considering a two-dimensional Cartesian coordinate system, where x designates the radial and z the vertical space direction. Some geometry data are listed in the table below.

Table I – Geometry data of winding

Variable	Unit	Value
Inner radius of winding	m	0.887
Outer radius of winding	m	1.059
Bottom of winding	m	0.2
Top of winding	m	2.2655
No. of coils	-	68

3.2. Grids

The following table lists some properties of the block-structured, hexahedral grids employed in our simulations. The 1st of these grids is used for the hydrodynamic runs while the 2nd grid includes a representation of the winding in addition.

Table 2 – Data of block-structured, hexahedral grids

Variable	Unit	Hydrodynamic runs	Coil representation
No. of blocks	-	259	55
No. of nodes	-	1464960	3475584
No. of fluid nodes	-	1464960	1464960
Node lengths	mm	0.16 – 0.97	0.16 – 0.97

The table shows only data of the finest geometric multi-grid level. However, 3 grid levels are used to investigate the influence of the discretisation error. Furthermore, they allow for Richardson extrapolation [12], to estimate grid independent solutions.

3.3. Boundary conditions

We consider oil velocities at the inlet of 1, 5, and 10 mm/s. The oil inlet temperature is T_i = 343 K. In the conjugate heat transfer simulation, adiabatic conditions are assumed at all computation domain boundaries, except the in- and outlet. Moreover, in the conjugate heat transfer run the power density of the losses in the coils is P_d = 40.29 kW/m^3.

3.4. Properties of oil flow and estimation of boundary layer thickness

The following table lists some general properties of the oil flow. These were calculated with the half length of the longest horizontal oil flow path in the sealing ring of 0.114 m as characteristic length *l*, the highest considered oil inlet velocity of 10 mm/s, and the oil inlet temperature of 343 K.

Table 3 – Properties of oil flow and boundary layer thickness

Variable	Unit	Value
Reynolds number	-	300
Prandtl number	-	50.85
Hydrodynamic boundary layer thickness	mm	6.6
Thermodynamic boundary layer thickness	mm	1.8

The upper limits of the hydro- and thermodynamic laminar boundary layer thickness are estimated by

$$\delta_h \propto \frac{l}{\sqrt{R}}; \quad \delta_t \propto \delta_h \, Pr^{-\frac{1}{3}} \,, \tag{5}$$

[10]. Here *R* is Reynolds' number and *Pr* Prandtl's number. According to [17], for the flow along a plate the transition from laminar to turbulent boundary layer flow occurs between R = 3.5 * 10^5 and 10^6. The location depends on the free stream degree of turbulence (fsti). As the Reynolds number of the oil flow in the transformer winding is much below the critical range, we assume that it is laminar.

Comparison of table 2 and table 3 shows that our grids are fine enough to adequately resolve the hydrodynamic and thermal boundary layers.

3.5. Results of hydrodynamic simulations

In our hydrodynamic simulations a steady state is established. The oil temperature is the inlet temperature of 343 K in the entire computation domain. The figures in this section all refer to the run with an oil inlet velocity of 10 mm/s.

The Cartesian components of the oil velocity in the static ring labyrinth below the winding are shown in the figure below. As a result of the low oil velocity, the meandering flow is more pronounced at the inner than at the outer sides of the curves. A similar result is obtained in the upper labyrinth.

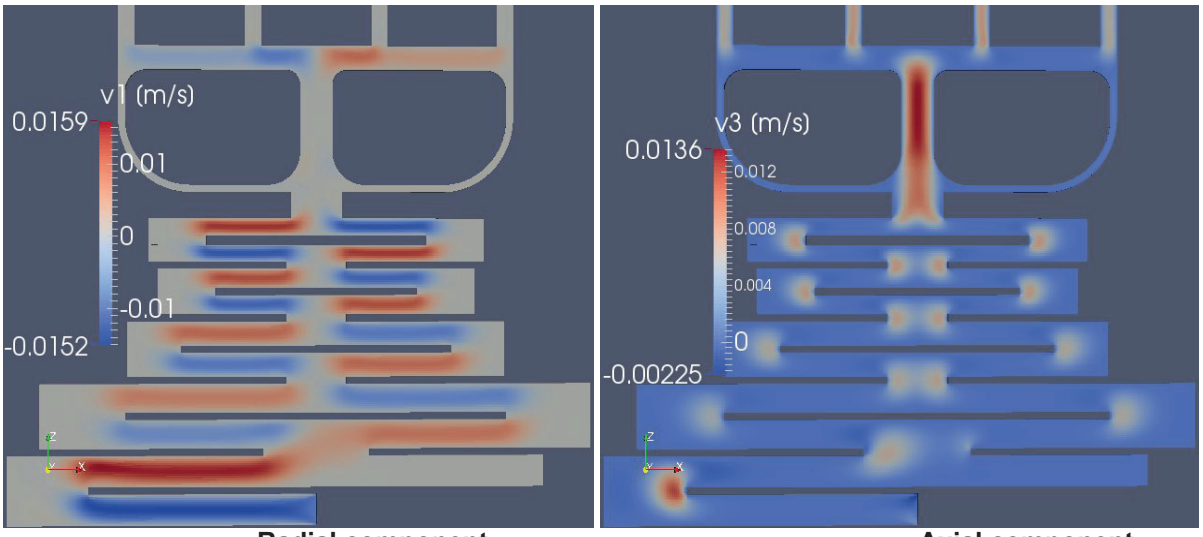

Radial component **Axial component**

Figure 1 – Velocity in lower labyrinth of hydrodynamic simulation

The next figure shows that the calculated velocity in the winding is most pronounced in the axial oil channels and oriented almost exclusively vertically. Compared to the axial oil flow, the flow in the radial channels is negligible.

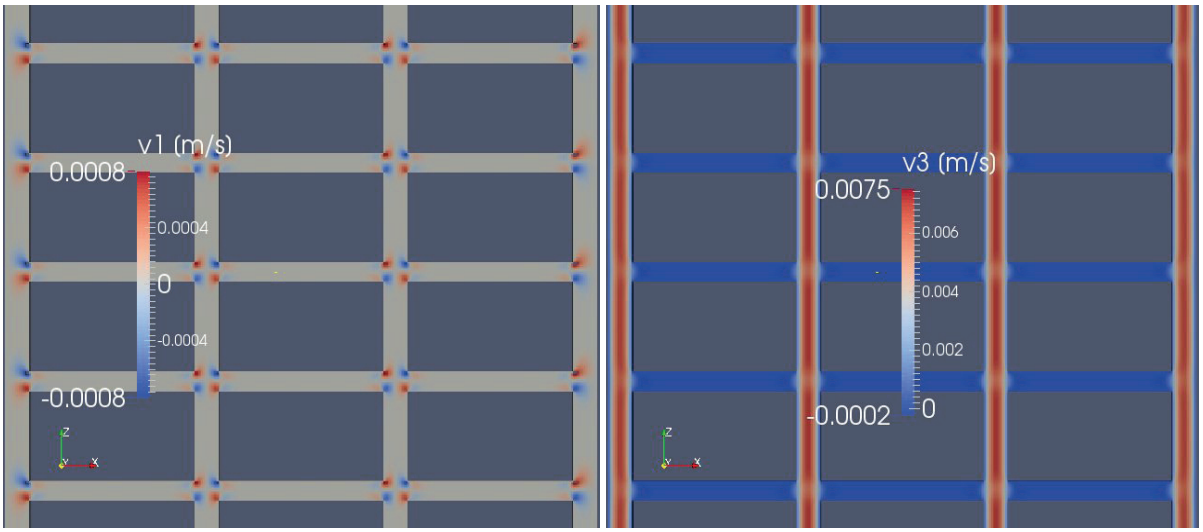

Radial component **Axial component**

Figure 2 – Velocity in winding section of hydrodynamic simulation

The related spatial distribution of the pressure variable of the oil in the entire model and at the labyrinth below the winding is shown in the following figure. In hydrodynamic runs our pressure variable

$$p_g := p - \rho_0 \, g_i \, (z_{\max} - z); \;\; \rho_0 := \rho(\, T_0 \,) = 841.2 \frac{kg}{m^3}. \tag{6}$$

omits the hydrostatic contribution to the pressure.

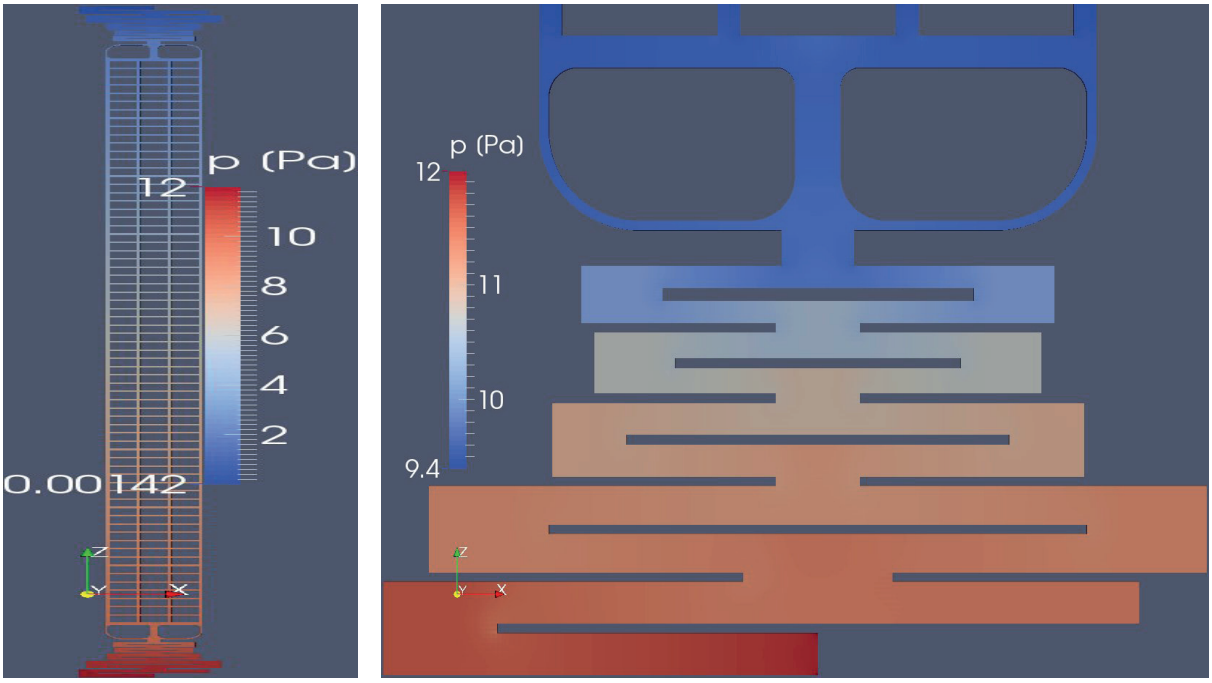

Entire model **Labyrinth below winding**

Figure 3 – Pressure variable of hydrodynamic simulation

The following table provides a list of the calculated oil flow induced pressure loss, as a function of the inlet velocity. It shows, as well as figure 4, that the dependence of the pressure loss on the inlet velocity is almost linear. Linear dependence corresponds to Hagen Poisseuille flow [10].

Table 4 – Pressure loss in hydrodynamic simulations

Inlet velocity [mm/s]	Pressure loss [Pa]
1	1.146
5	5.811
10	11.91

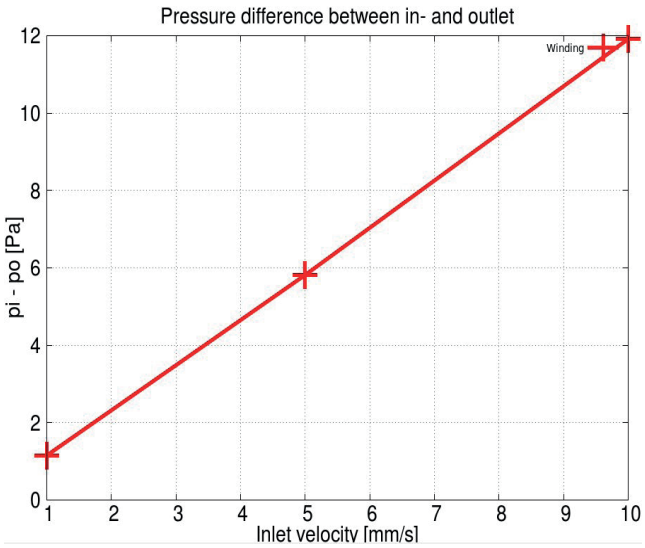

Figure 4 – Pressure loss in hydrodynamic simulations

3.6. Results of conjugate heat transfer simulation

In our conjugate heat transfer run with the coil model, a spatially constant heat source is applied inside the coils, see section 3.3. Unlike a heat flux boundary condition at the interface between coils and oil, this ensures proper matching of the temperature distribution in the oil and the heat flux at the interface.

As a result of the gravitational acceleration and the temperature dependent density of the oil, the generated heat leads to buoyancy forces and natural convection in the oil. For this reason, here we consider only the high inlet velocity of 10 mm/s. According to energy conservation, at this inlet velocity the average outlet oil temperature at the thermal steady state is

$$T_o = T_i + \frac{P}{\dot{m}\, c_p} = 386.16\,K\,. \tag{7}$$

Here P is power of losses, $\dot{m}$ mass flow, and c_p specific heat at constant pressure. In our simulation, there are varying oil flow patterns during the iterations and the residual of the specific enthalpy is not converging. This raises the presumption that there is no hydrodynamic steady state. The calculated temperature in the oil and the coils is shown in the figure below. The right part of the figure indicates that there are hot oil locations adjacent to the coils. These hot regions change their location during the iterations. This is due to the lack of axial flow barriers, that hampers the development of a steady, preferred direction of the oil flow.

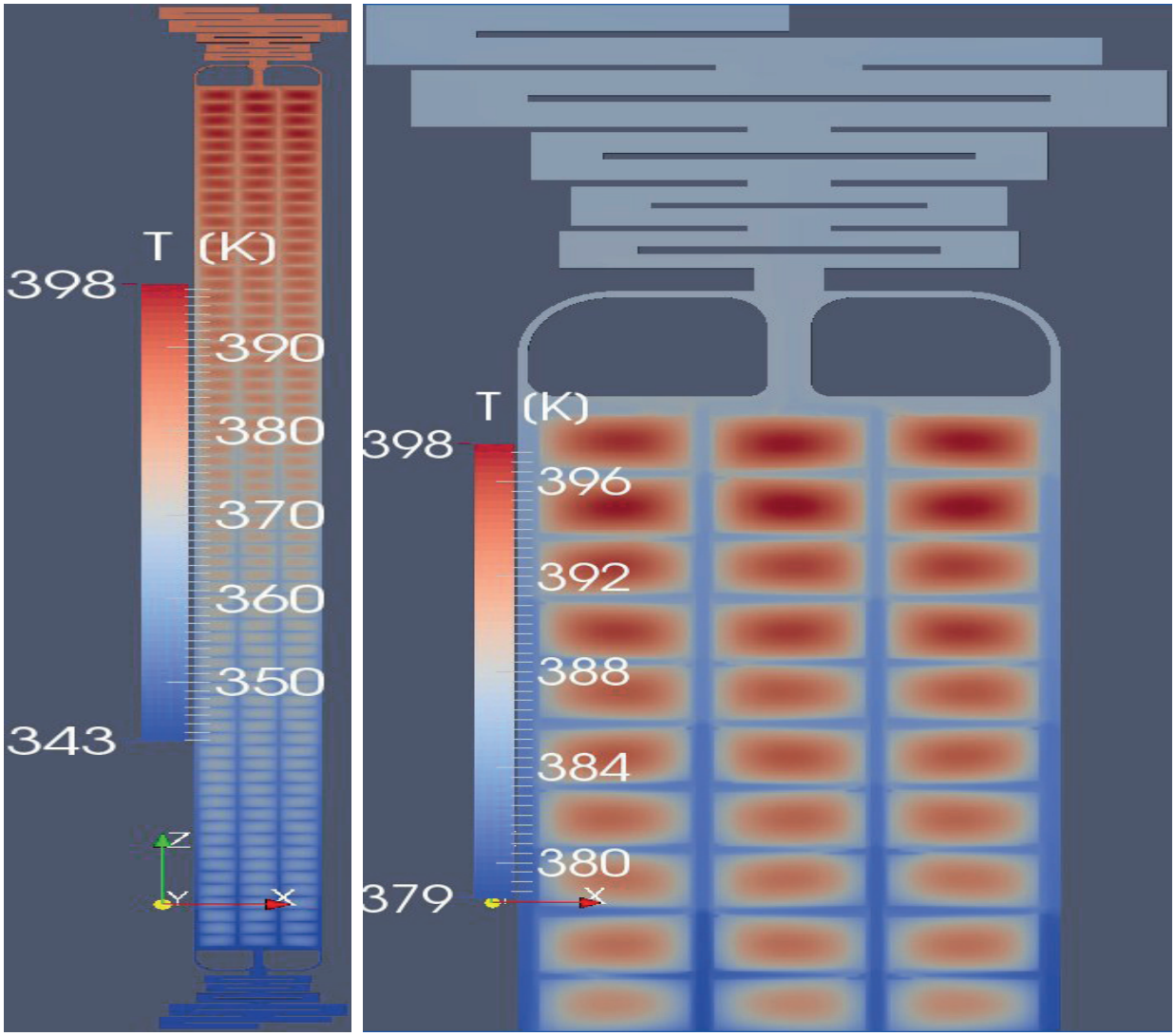

Entire model **Upper winding and labyrinth**

Figure 5 – Oil temperature of conjugate heat transfer simulation

As a result of our mixture material properties the heat conductivity in the coils is low. For this reason, there is a smooth temperature variation in the coil and the maximum coil temperature is high. However, as the goal of this simulation is the temperature dependent hydrodynamics, the coil temperature is of minor importance. The coil in our model is just a means to guide the heat flux from the heat source to the colder sections of the surrounding oil.

In the right part of the figure we see that the oil temperature is not constant along the radial channels. This is related to the direction of the flow. Since the flow does not reach a steady state there is also no local thermal equilibrium in the oil. The figure also shows that the oil temperature at the outlet is about 386 K. This agrees with the energy balance (7). For this reason, a global thermal equilibrium is achieved.

The next figure shows the related Cartesian velocity components at the upper section of the geometry model.

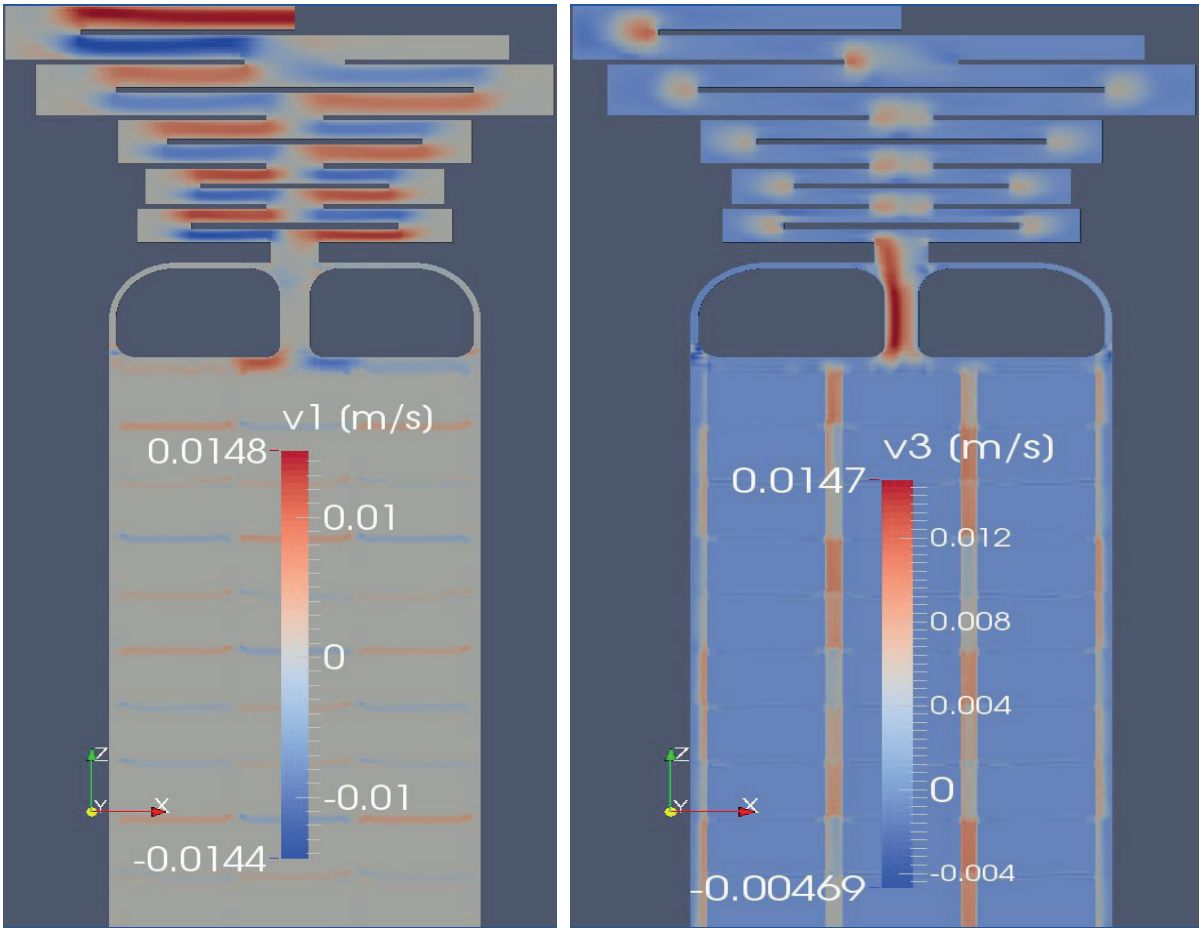

Radial component **Axial component**

Figure 6 – Cartesian velocity components of conjugate heat transfer simulation

As mentioned before, the velocity in the winding varies during the iterations. At some iteration, e.g., the vertical velocity at certain location in an axial oil channel may be directed upward, while the flow goes down at a later iteration. Moreover, comparison of Fig. 2 and Fig. 6 shows that the velocity is higher and much more uneven than in the hydrodynamic simulation.

The higher irregularity of the flow could lead to a higher pressure loss, compared to the hydrodynamic case. However, as a result of strong heat sources and low inlet velocity, this flow is dominated by buoyancy rather than a pressure gradient caused by wall friction. The pressure merely acts as a Lagrangian multiplier that assures that the velocity is divergence-free. In order to maintain the outlet mass flow at the same low level than the inlet mass flow, the pressure variable (6) in this application increases from inlet to outlet, as shown in the following figure. Our pressure variable omits the hydrostatic contribution to the pressure in hydrodynamic simulations and causes the negative values in the figure. If heat transfer is involved, there is no such simple method to remove the hydrostatic part. The pressure itself, however, is higher at the inlet than at the outlet.

Since the buoyancy forces efficiently accelerate the flow, they may cause a higher inflow velocity than specified in our simulation, unless a high friction (e.g., caused by an inlet nozzle) prevents this.

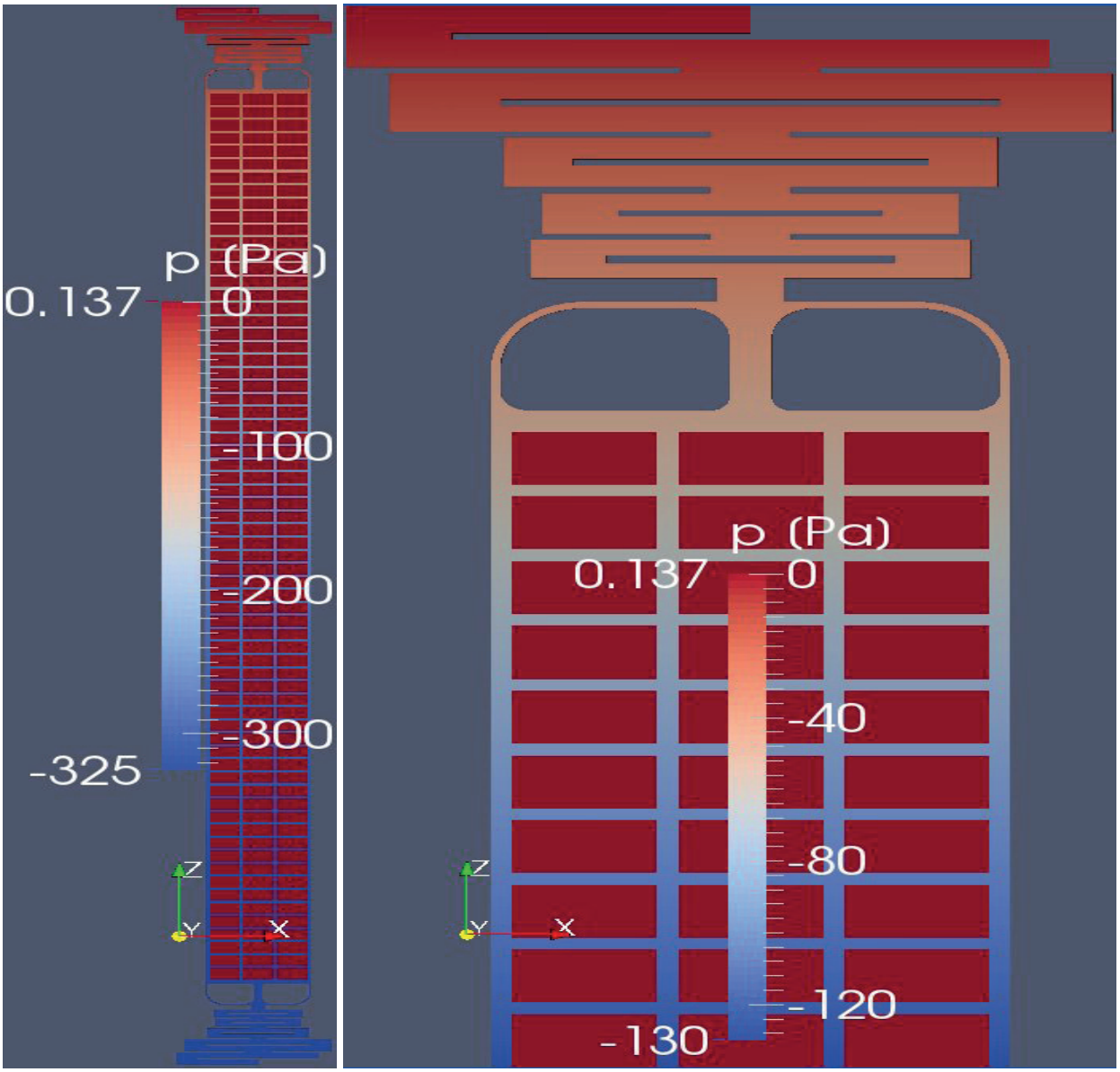

Entire model **Upper winding and labyrinth**

Figure 7 – Pressure variable of conjugate heat transfer simulation

4. SUMMARY AND CONCLUSIONS

We analysed the pressure loss of mineral oil flow in the valve winding of a HVDC transformer with the Siemens in-house CFD code UniFlow. In the hydrodynamic simulations a steady state is established and the pressure loss is an almost linear function of the inlet velocity. In the run involving heat transfer, the high buoyancy forces hamper the development of a steady state and the possibility to calculate a flow induced pressure loss.

The presented results indicate that UniFlow is a useful tool to analyse the thermal design of transformers. It can be used to investigate advantages and disadvantages of design features as well as to perform design optimisation.

In addition to the results shown in this paper, the temperature of insulation materials in a device subject to fluid flow may be a major result of a simulation. Furthermore, the thermal design of cast resin

transformers can be studied, including radiant heat transfer between core, windings, and radiation cylinders. This is demonstrated, e.g., in [18]. Other applications are related to detailed analyses on segments of disc windings with respect to, e.g., modelling of material compositions, width of oil channels, etc.. Another field of application are oil flows in transformer cores. Moreover, combined oil and air flows are analysed in the context of fin type distribution transformers. This is aimed at optimisation of the thermal efficiency of the fins and other tasks. Furthermore, combined oil and air flows in radiators can be investigated.

In addition to steady state analyses, transient processes are investigated. One interesting type of transient occurs at the cold start of a transformer. This matters in particular for oil transformers where the dynamic viscosity is very high at low temperatures, especially for ester fluids.

REFERENCES

[1] Torriano, F., Pichler, P., Chaaban, M., "Numerical investigation of 3D flow and thermal effects in a disc-type transformer winding“, Applied Thermal Engineering, 40, pp. 121-131, 2012

[2] Jiao, Y., "CFD study on the thermal performance of transformer disc windings without oil guides“, KTH School of Industrial Engineering and Management, EGI-2012-089MSC EKV915, Stockholm, Sweden, 2012

[3] Smolka, J., Nowak, A. J., "Experimental validation of the coupled fluid flow, heat transfer and electromagnetic numerical model of the medium power dry-type electrical transformer“, Int. J. Thermal Sciences, 47, pp. 1393-1410, 2008

[4] Smolka, J., Biro, O., Nowak, A. J., "Numerical simulation and experimental validation of coupled flow, heat transfer and electromagnetic problems in electrical transformers“, Arch. Comput. Methods Eng., 16, pp. 319-355, 2009

[5] Fonte, C. M. et. al., "CFD analysis of core-type power transformers“, CIRED, 21st Intl. Conf. on Electricity Distribution, paper 0361, Frankfurt, Germany, 6.-7. 2011

[6] Gastellurrutia, J. et. al., "Numerical modelling of natural convection of oil inside distribution transformers“, Applied Thermal Engineering, 31, pp. 493-505, 2011

[7] Baldwin, B. S., Lomax, H., "Thin layer approximation of and algebraic model for separated turbulent flows“, AIAA-paper, 78-0257, 1978

[8] Drela, M., "MISES implementation of modified Abu-Ghannam/Shaw criterion“, MIT Aero-Astro, Boston, MA, USA, February 1995

[9] Mayle, R. E., "The role of laminar-turbulent transitions in gas turbine engines“, ASME Journal of Turbomachinery, 13, pp. 509-537, 1991

[10] Landau, L. D., Lifshitz, E. M., "Course of theoretical physics, vol. 6 : Fluid mechanics“, Pergamon Press, Oxford, UK, 1989

[11] Baehr, H. D., Stephan, K., "Heat and mass transfer“, Springer-Verlag, Berlin, Germany, 2006

[12] Ferziger, J. H., Peric, M., "Computational methods for fluid dynamics“, Springer-Verlag, Berlin, Germany, 1999

[13] Van Doormal, J. P., Raithby, G. D., "Enhancements of the SIMPLE method for predicting incompressible flows“, Numer. Heat Transfer, 7, pp. 147-163, 1984

[14] Issa, R. I., "Solution of implicitly discretized fluid flow equations by operator splitting“, J. Comp. Phys., 62, pp. 40-65, 1986

[15] Trottenberg, U., Oosterlee, C. W., Schüller, A., "Multigrid“, Academic Press, New York, USA, ISBN 012701070X, 2001

[16] Notay, Y., "An aggregation-based algebraic multigrid method“, Electronic Transactions on Numerical Analysis, 37, pp. 123-146, Kent State University, ISSN 1068-9613, 2010

[17] Schlichting, H., "Boundary-layer theory“, McGraw-Hill, New York, USA, 1979

[18] Wittmaack, R., "Thermal design of power transformers via CFD“, 11th World Congress on Computational Mechanics (WCCM XI), Barcelona, Spain, July 21-25, 2014